Applied Catalysis B: Environmental 201 (2017) 105–118

Contents lists available at ScienceDirect

Applied Catalysis B: Environmental

journal homepage: www.elsevier.com/locate/apcatb

The influence of p-type Mn_3O_4 nanostructures on the photocatalytic activity of ZnO for the removal of bromo and chlorophenol in natural sunlight exposure

M. Tariq Qamar[a,b], M. Aslam[a], Z.A. Rehan[b,c], M. Tahir Soomro[a], Jalal M. Basahi[d], Iqbal M.I. Ismail[a,b], Talal Almeelbi[e], A. Hameed[a,f,*]

[a] Centre of Excellence in Environmental Studies (CEES), King Abdulaziz University, Jeddah 21589, Saudi Arabia
[b] Chemistry Department, Faculty of Science, King Abdulaziz University, P.O. Box 80203, Jeddah 21589, Saudi Arabia
[c] Centre of Excellence in Desalination Technology, King Abdulaziz University, Jeddah 21589, Saudi Arabia
[d] Department of Water Resources Sciences and Management, Faculty of Meteorology, Environment and Arid Land Agriculture, King Abdulaziz University, Jeddah 21589, Saudi Arabia
[e] Department of Environmental Sciences, King Abdulaziz University, Jeddah 21589, Saudi Arabia
[f] National Centre for Physics, Quaid-e-Azam University, Islamabad, 44000, Pakistan

ARTICLE INFO

Article history:
Received 7 April 2016
Received in revised form 20 July 2016
Accepted 2 August 2016
Available online 2 August 2016

Keywords:
Sunlight photocatalysis
4-Bromophenol
4-Chlorophenol
Mn_3O_4 modified ZnO

ABSTRACT

The issues of low photocatalytic activity and dissolution of ZnO in natural sunlight exposure were addressed by implanting *p-type* Mn_3O_4 on its surface. The optical analysis revealed the composite nature and suppression of exciton excitons recombination whereas the cyclic voltammetry, electrochemical impedance spectroscopy (EIS) and chronopotentiometry substantiated the elimination of photocorrosion respectively, low charge transfer resistance and better charge retention ability for the as-synthesized composites. The Mott-Schottky analysis by staircase potential impedance spectroscopy (SPIES) verified the *p-n* nature while the measurement of flat band potential (V_{fb}) predicted the suitability of the band potentials for the enhanced generation of reactive oxygen species (ROS). The structure and morphology of the Mn_3O_4-ZnO composites were evaluated by x-ray diffraction (XRD) and field emission electron microscopy (FESEM) whereas the fine structure analysis was performed by high-resolution transmission electron microscopy (HRTEM) analysis that revealed the discrete fringe patterns of *p-type* Mn_3O_4 and ZnO in composites. The x-ray photoelectron spectroscopy (XPS) verified the simultaneous existence of Mn^{2+} and Mn^{3+} in Mn_3O_4 nanoparticles. Compared to pure ZnO, due to the existence of charge transfer synergy between the *p-type* Mn_3O_4 and *n-type* ZnO, the composites with moderate Mn_3O_4 loadings exhibited marked activity for the removal of stable pollutants like 4-bromo and 4-chlorophenol in natural sunlight exposure. The correlation of the findings from various analytic tools of chemical analysis such as high-performance liquid chromatography (HPLC), ion chromatography (IC), total organic carbon (TOC) measurements and GC–MS analysis revealed the persuasive role of Cl and Br groups in regulating the degradation process. The composite catalyst exhibited excellent stability and reproducible activity in the repeated scans.

1. Introduction

The use of sunlight in photocatalytic processes as excitation source can lead to an economically viable and cost-effective solution of water purification, however, demands the development of sunlight active photocatalysts. Among the existing metal oxides, Zinc oxide, with the extended absorption cross-section in the visible region, can be a suitable choice in this regard, however, largely disregarded as photocatalyst due to high recombination rate of excitons and instability during photocatalytic processes [1,2]. The promising optical properties and photocatalytic activity with significantly high fluorescence emissions succeeding that of TiO_2 along, narrates its potential to be valuable photocatalyst after being subjected to suitable surface modification to address simultaneously the associated issues of recombination and

* Corresponding author at: Centre of Excellence in Environmental Studies (CEES) King Abdulaziz University, Jeddah, Saudi Arabia.
E-mail addresses: hameedch@yahoo.com, ahfmuhammad@gmail.com, afmuhammad@kau.edu.sa (A. Hameed).

http://dx.doi.org/10.1016/j.apcatb.2016.08.004
0926-3373/

photocorrosion without disturbing the inherent activity. Several surface modifications such as metal impregnation, metal oxide coating, and composite formation have been proposed and investigated so far to address the above-mentioned issues [3–5]. Among the proposed modifications with respect to photocatalysis, the composite formation is a well-established tool to achieve the required goals [6–8]. In this respect, few studies have been reported so far using a composite of ZnO with transition metal oxides for the degradation and mineralization of toxic organic pollutants under illumination of sunlight [2,9–12].

Organic pollutants, with established hazards to living beings, mainly the feedstock and byproducts of many industries, not only pollute surface water but also contaminate the ground water. The halogenated derivatives of phenols due to their ample use in a variety of industries, considerable occurrence in polluted water, high solubility and strong resistance towards removal; have attained much more attention [13–16]. With the associated features of the possibility of the use of ever-renewable sunlight (44–46% visible and 3–5% UV photons), generation of ROS, inexpensive and effortlessly recoverable photocatalysts, heterogeneous photocatalysis has emerged as a power tool for environmental remediation especially water decontamination [17–23]. Although a number of researchers investigated the photocatalytic removal of chlorophenols, however, artificial light sources were used as excitation sources in almost all the studies [24] and lack the detailed investigation i.e. the identification of intermediates, TOC removal, plausible mechanism etc. The investigations on the photocatalytic removal of bromo derivatives especially 4-bromophenol in sunlight exposure are rare.

The preliminary stage disclosure of the suitability and compatibility of manganese (Mn) based oxides with ZnO for the photocatalytic applications motivated us to design a detailed investigation on the synthesis, characterization and photocatalytic activity of the Mn_3O_4 altered ZnO [25–30]. The composites of Mn_3O_4 (ranging from 0.5% to 10%) and ZnO (Fixed amount) were synthesized initially by loading the hydrogel of Mn^{2+} ions on pre-synthesized ZnO and finally converted to Mn_3O_4-ZnO composites by calcination. The morphology and particle size of the deposited particles were controlled by the addition of surfactant. The optical properties of the synthesized composites were investigated by using UV–vis diffuse reflectance spectroscopy (DRS), photoluminescence (PL) while the structural and chemical characterization was carried out by X-ray diffraction (XRD) and X-ray photoelectron spectroscopy (XPS). The morphology and texture of the materials were assessed by field emission electron microscopy (FESEM) and HRTEM. The variations in the semiconducting properties of ZnO, the flat band potential, electron transport, and charge retention ability of the synthesized powders were investigated by staircase potential impedance spectroscopy (SPIES), electrochemical impedance spectroscopy (EIS) and chronopotentiometry (CP) whereas the stability of the materials under illumination was assessed by cyclic voltammetry (CV). The photocatalytic activity of the materials was evaluated for the removal of 4-bromo and 4-chlorophenol in sunlight exposure. The progress of removal and mineralization was monitored by HPLC and TOC where the release of released ions was monitored by ion chromatography (IC). Selected samples were subjected to GCMS for the identification of intermediates.

2. Experimental details

The composites loaded with 0.5%, 1%, 3%, 5% and 10% Mn_3O_4 with respect to the weight of ZnO were synthesized by dissolving the stoichiometric amounts of $Mn(NO_3)_2{\cdot}4H_2O$ (Sigma-Aldrich, 99.5%) in 200 ml of de-ionized water. Prior to hydrolysis, the metallic solution was stirred with Triton X-100 (used as a surfactant) at 100 °C and then the solution containing metals was hydrolyzed by dropwise addition of 0.5 M KOH (Sigma-Aldrich, 99.5%) with vigorous stirring till pH 8. The precisely weighed amount of pre-synthesized ZnO detailed elsewhere [1,31] was added in the solution. The $Mn(OH)_2$ hydrogel/ZnO suspension was heated at 100 °C for 5 h until the formation of fine precipitates and filtered. The excessive KOH and surfactant were removed by successive washing with of deionized water and 50:50 ethanol-acetone mixture to ensure the complete removal of surfactant and neutralize the pH. The collected precipitates were dried, crushed, and calcined in a muffle furnace at 400 °C for 4 h at a heating and cooling rate of 10 °C/min. The solid-state absorption and diffuse reflectance spectra of the materials were recorded by a Perkin Elmer UV–vis diffuse reflectance spectrophotometer (Lambda 650) in the wide range of 190–900 nm. The band gaps of the materials were evaluated by applying the Kubelka-Munk transformation on%R data. The photoluminescence (PL) and Raman spectra of the materials were acquired by a fluorescence spectro-fluorophotometer, RF-5301 PC, Shimadzu, Japan at an excitation wavelength of 200 nm and a DXR Raman Microscope, Thermo Scientific, USA, equipped with 532 nm laser as the excitation source at 6 mW power, respectively. The XRD patterns of the pure and as-synthesized powders were recorded by Scintag XDS 2000 diffractometer, equipped with a Cu *Kα* radiation source, in 0–90° range. The XPS profile of synthesized powder was assimilated in the binding energy range of 0 eV to 1100 eV by X-ray Photoelectron Spectrometer (PHI 5000 VersaProbe II, ULVAC-PHI Inc.). The oxidation states of Mn and Zn were estimated by applying curve fitting and comparing the data with standard values. The morphology of the synthesized powder was inspected by Field Emission Scanning Electron Microscope (FEI, Quanta FEG 450, Quorum Q150R ES, Quorum technologies Ltd. Ashford. Kent. England) at a voltage of 30 kV and High-Resolution Transmission Electron Microscope (JEM-2100 JEOL, USA) at different magnifications. In addition, TEM grids were prepared by putting a 5 μl dilute slurry of the material onto a 200 mesh copper grid.

The electrochemical behavior and stability of the Mn_3O_4-ZnO composites and ZnO, in the dark and under illumination, were carried out by cyclic voltammetry (CV), electrochemical impedance spectroscopy (EIS) and chronopotentiometry (CP). For CV, EIS and charge-discharge analysis, a VSP multi-channel potentiostat (Biologic Science Instrument, USA) equipped with Ec-lab software and three electrode system namely; glassy carbon (GC), platinum and Ag/AgCl saturated electrodes as working, counter and reference electrodes, respectively. For the modification of GCE (working electrode), a sonicated dispersion of catalyst in chloroform was coated at the surface. The fitting of EIS Nyquist plots was performed by Zfit (Ec-lab software, Bio-logic Science Instruments, USA). Except for CV analysis which was performed by using 0.1 M (pH 9) phosphate buffer, 0.1 M (pH 7) phosphate buffer and 0.1 M (pH 2) phosphate buffer electrolyte to evaluate the stability under varying pH environment, all the other measurement were executed in 0.1 M KCl solution. The Mott-Schottky analysis was performed by sweeping the potential in the range of −1.5–1.5 V versus saturated calomel electrode (SCE) with an AC frequency of 1 kHz and an amplitude of 10 mV, both in the dark and under illumination. The working electrodes were prepared by casting off 10 μl of the 2:1 (2 mg in 1 ml of 0.1% Nafion solution) photocatalysts water suspension onto a glassy carbon electrode. A 50-W halogen lamp was used as a source for the measurements under illumination.

The photocatalytic performance of Mn_3O_4-ZnO composites and pure ZnO powders was assessed in a complete spectrum of sunlight illumination by exposing 200 ml of 4-bromophenol (4-BP, 50 ppm) and 4-chlorophenol (4-CP, 50 ppm) containing the optimized quantity (75 mg/L) of a respective photocatalyst in a Pyrex® glass reactor. The dimensions and surface area of the glass reactor were 15.5(diameter) × 2.5(height) and 189 cm^2 respectively. Prior

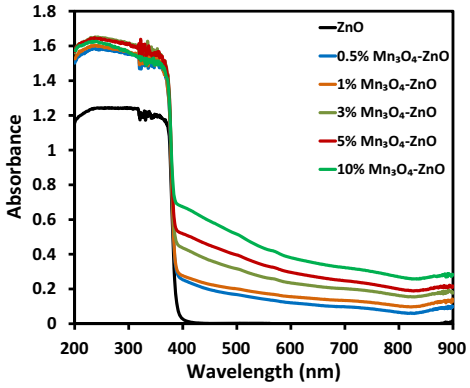

Fig. 1. The comparison of the solid state absorption spectra of the pure and Mn_3O_4 loaded ZnO composites.

to exposure, the catalyst/substrate suspension was kept in the dark to establish adsorption-desorption equilibrium. Additionally, the photolysis of substrates was also investigated. During the exposure ($1000 \pm 100 \times 10^2$ lx) samples were drawn at regular intervals and subjected to HPLC (HPLC, SPD-20A, Shimadzu Corporation, Japan), TOC (TOC-VCPH) total carbon analyzer, Shimadzu Corporation, Japan and IC (Thermo scientific, USA, ion chromatograph, Dionex (ICS–5000 + EG) Eluent Generator) analysis for the monitoring of degradation, mineralization and estimation of released ions respectively, during the photocatalytic process. Selected samples were analyzed by GC–MS (Shimadzu Corporation, Japan, Shimadzu-QP 2010 Plus) equipped with a Rtx-1 capillary column and helium (He) as a carrier gas, for the identification of intermediates formed during the photocatalytic degradation process.

3. Results and discussion

As mentioned in the experimental details, the Mn_3O_4 loaded ZnO composites were synthesized by loading the solid hexagonal ZnO with various proportions of *p-type* Mn_3O_4. The morphology of the synthesized particles and the even distribution at the surface of ZnO was controlled by the use of surfactant. The characterization and photocatalytic activity of the synthesized composites are discussed below.

The comparison of the solid state absorption spectra of pure and Mn_3O_4 loaded ZnO composites, in the spectral range of 200–900 nm, is presented in Fig. 1, where compared to pure ZnO, a significantly enhanced absorption of composites, in 450–800 nm range, is observable. The magnitude of the absorption increased with the increasing surface density of Mn_3O_4 entities and signified

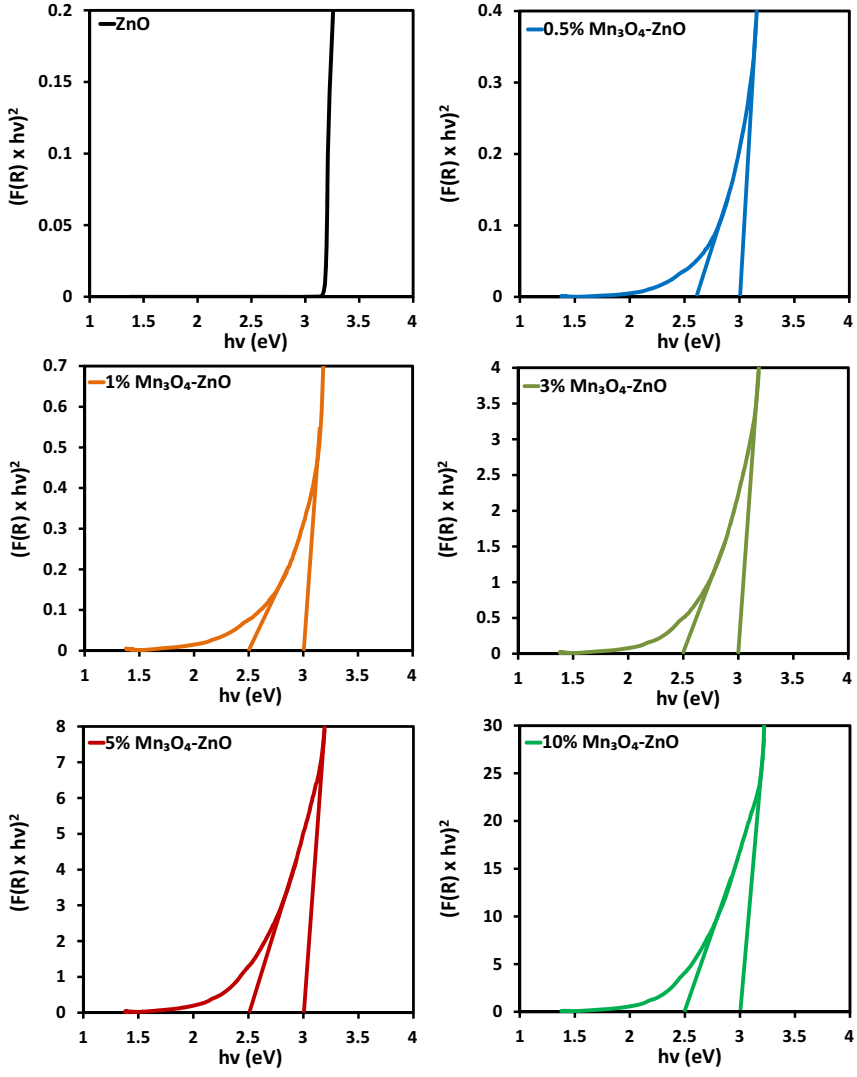

Fig. 2. The graphical evaluation of the direct band gaps of Mn_3O_4-ZnO composite powders in comparison to pure ZnO.

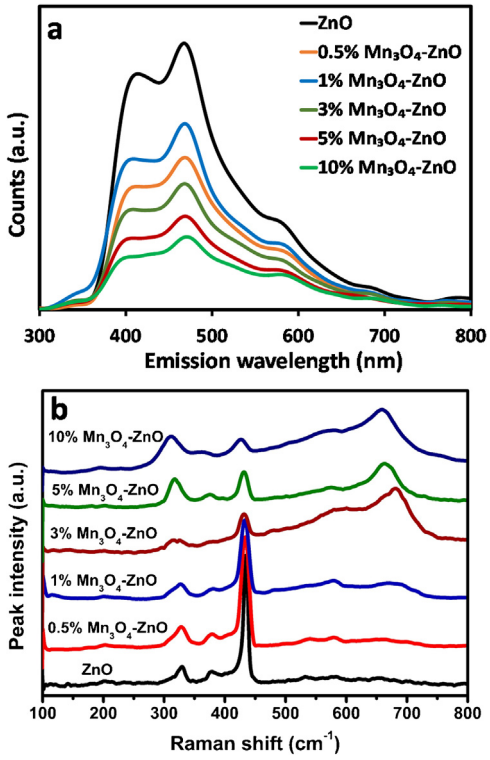

Fig. 3. The comparison of the (a) PL spectra at an excitation wavelength of 325 nm and (b) Raman shift spectra of pure and Mn_3O_4 modified ZnO composites.

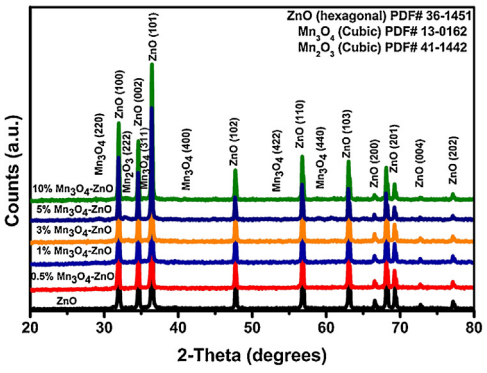

Fig. 4. The comparison of the XRD patterns of pure and Mn_3O_4 loaded ZnO composites in the 2θ range of 20° to 80°.

the contributory role of a Mn_3O_4 component of the composites in the better absorption of photons in the visible region. Interestingly, a mild shift in the absorption edges of the ZnO component of the composites was also witnessed.

The graphical evaluations of the band gaps extracted by plotting $(F(R) \times h\nu)^2$ versus photon energy ($h\nu$) for pure ZnO and Mn_3O_4 loaded ZnO composites are presented in Fig. 2. The evaluated bandgap of ~3.2 eV for pristine ZnO was in sound agreement with the literature values [31,32]. The appearance of dual distinct band energies for 0.5%, 1%, 3%, 5% and 10% Mn_3O_4 modified ZnO evinced the composite nature of the synthesized material. Additionally, as compared to pure ZnO, a mild red-shift of ~0.2 eV in the band edge position of ZnO component of the composites was noticed. The induction of the Mn^{2+} and Mn^{3+} entities along with Zn^{2+} states at the surface is the probable reason for the effect. The band edge of ~2.5 eV for the Mn_3O_4 component was consistent for all the composites except for 0.5% Mn_3O_4 loaded ZnO, where probably the lower Mn_3O_4 loading resulted in the relatively higher bandgap energy of ~2.65 eV. With the minor variations, the evaluated bandgap energies of a Mn_3O_4 component of the composites were in accordance with the literature values [33].

Fig. 3 (a) shows the comparison of the PL spectra of pure ZnO and the synthesized composites at an excitation wavelength of 200 nm, where a significant decrease in the emission intensities of composite materials compared to pristine ZnO is observable. Zinc oxide (ZnO) is a highly fluorescent material with the characteristic bands centered at ~412.9 nm and ~471.5 nm. The band between 370 and 420 nm with the maxima at ~412.9 nm represents the de-excitation from the conduction band to the valence band whereas the broad-band between 440 and 500 nm corresponds to the delayed emissions due to trapped electrons in oxygen vacancies [9]. The successive decrease in luminescence intensities of characteristic bands of ZnO with the increasing surface concentration for the composites established the existence of the charge transfer synergy between the of Mn_3O_4 and ZnO components that lead to an extended lifetime of the excited states.

The comparison of the Raman spectra of pure and Mn_3O_4 modified ZnO is presented in Fig. 3(b). In the current study, the surface changes in ZnO with the accumulation of Mn_3O_4 were assessed by targeting the Raman active modes at ~330.03 cm^{-1} and ~434.65 cm^{-1}. The appearance and origin of these bands are well documented [31]. The decrease in the intensity of high band (~434.65 cm^{-1}), that corresponds to vibrational modes of Zn-O^- surface groups, was attributed to the formation of Zn-O-Mn type surface structures that restrict the vibrations with the induction of rigidity. Additionally, besides the significant decrease in the intensity, a mild shift of ~4 cm^{-1} in the peak position was also witnessed. Furthermore, an additional band in 650 cm^{-1} to 700 cm^{-1} region due to surface Mn-O^- was also witnessed for the composites with 1% or higher Mn_3O_4 loading. The intensity of the band increased with the increasing surface concentration of Mn_3O_4 whereas a successive decrease was noticed in the principal bands of ZnO.

Fig. 4 shows the comparison of the XRD patterns of bare ZnO and Mn_3O_4 loaded ZnO. The major reflections of pure ZnO appeared at the 2θ values of 31.9°, 34.6°, 36.5°, 47.7°, 56.8°, 63.1°, 66.5°, 68.1°, 69.2°, 72.7° and 77.1° corresponding to (100), (002), (101), (102), (110), (103), (200), (112), (201), (004) and (202) *hkl* indices, respectively, matched with hexagonal ZnO (JCPDS 36-1451). An observable decrease in the intensity of above-mentioned reflections was noticed with the increasing surface density of Mn_3O_4. Besides the reflections of ZnO, the additional reflections at 2θ values of 29.8°, 35.7°, 42.8°, 53.5° and 59.4° corresponding to (220), (311), (400), (422), and (440) planes of cubic Mn_3O_4 (JCPDS# 13-0162) were also identified. The observed reflections were in sound agreement with the observed literature values [34]. Additionally, for the samples with higher loading i.e. 5% and 10% Mn_3O_4-ZnO composites, the expected minor reflections due to Mn_2O_3 with the cubic phase (JCPDS 41-1442) were also witnessed. Based on the most intense reflection at 36.5° (%I = 100) a crystallite size of ~58.1 nm was evaluated for ZnO whereas 28.1 nm for Mn_3O_4. Although a mild decrease in the intensity of ZnO reflections was noticed with the increasing Mn_3O_4 loading, however, their sharpness and distinct texture reflected the well-defined crystal structure of ZnO with high crystallinity even after the loading of Mn_3O_4.

The typical wide angle XPS survey scan of 5% Mn_3O_4 loaded ZnO composite is shown in Fig. 5a, where the peaks corresponding to the binding energies of the core and splitted levels of the components of the composite i.e. Zn, Mn, and O are observable. The C1s peak was noticed at ~285.38 eV. For a comprehensive evaluation of oxidation states and the chemical environment of each, the splitted peaks corresponding to O1s, Mn2p and Zn2p were deconvoluted and fitted. As presented in Fig. 5b, the fitting of O1s spectra disclosed the presence of the multiple peaks of variable intensities

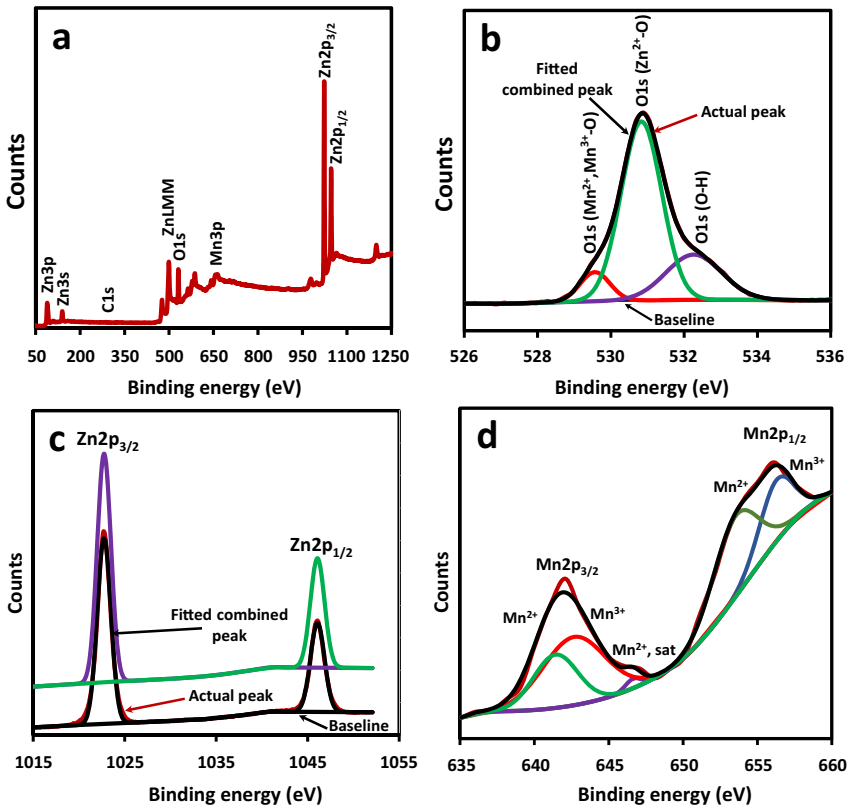

Fig. 5. The evaluation of (a) XPS survey of Mn_3O_4 loaded ZnO composite (b) O 1s levels (c) fitted Zn2p levels and (d) fitted Mn2p peaks.

and binding energies. The most intense major peak at ~531.1 eV represented the ZnO skeletal oxygen (Zn^{2+}–O) whereas the deconvoluted peaks at ~529.6 eV and ~532.5 eV specified the existence of oxygen attached to Mn (Mn^{2+}, Mn^{3+}–O) and the surface hydroxyl (O—H) groups, respectively, in the composite. The curve fitting of the splitted $Zn2p_{3/2}$ and $Zn2p_{1/2}$ resulted in the appearance of the corresponding peaks at ~1023.08 eV and ~1046.13 eV respectively, without any apparent change in the oxidation state of Zn during the synthesis (Fig. 5c). The observed values were in accordance with the previously reported values in the literature [31]. The fitting of the $Mn2p_{3/2}$ and $Mn2p_{1/2}$ splitted levels disclosed the probable existence of the multiple peaks corresponding to the 2+ and 3+ oxidation states of Mn (Fig. 5d). In the current study, the deconvolution of the splitted $Mn2p_{3/2}$ and $Mn2p_{1/2}$ levels, with the binding energy gap of ~12.5 eV, revealed the peak positions of Mn^{2+} ($2p_{3/2}$, $2p_{1/2}$) and Mn^{3+} ($2p_{3/2}$, $2p_{1/2}$) states at ~641.7 eV, ~654.3 eV and ~643.1, ~656.8 eV, respectively, whereas the characteristic Mn^{2+} satellite peak appeared at ~646.7 eV. Probably, due to the pronounced matrix effect by the ZnO, the observed values were slightly higher than the reported values for ZnO@Mn_3O_4 type core-shell structures [34]. The simultaneous appearance of the Mn^{2+} ($2p_{3/2}$, $2p_{1/2}$) and Mn^{3+} ($2p_{3/2}$, $2p_{1/2}$) peaks with the comparable intensities verified Mn_3O_4 as the combination of MnO and Mn_2O_3.

The comparison of the FESEM images of pure ZnO, pure Mn_3O_4, and Mn_3O_4 loaded ZnO composites at 120,000 × are presented in Fig. 6a–f, respectively. The hexagonal crystals of ZnO with distinct edges and a particle size distribution ranged between 10 nm to 70 nm are observable in Fig. 6a. The observed particles of Mn_3O_4 are the aggregates of smaller regular shaped units with the average particle size ranged between 10–20 nm (Fig. 6b). The growth of the Mn_3O_4 at the surface is observable with the increasing concentration without any noticeable change in the morphology of ZnO (Fig. 6c–f). The morphology of the deposited particles matched with that of pure Mn_3O_4 synthesized by the same route. For the 5% composite, the partial coverage of ZnO is observable whereas the majority surface coverage was witnessed for 10% Mn_3O_4-ZnO composite. A uniform distribution of the Mn_3O_4 particles was witnessed all over the surface of hexagonal ZnO without the selectivity for a particular face. The microstructure of the as-synthesized composites was further investigated by transmission electron microscopy (TEM) analysis at different magnification levels. The typical TEM image of the 3% Mn_3O_4-ZnO composite is presented in Fig. 7a, where the uniform distribution of Mn_3O_4 particles on the large hexagonal ZnO particles is obvious. In comparison to ZnO, the size of the Mn_3O_4 particles deposited at the surface was significantly smaller. As presented in Fig. 7b, the selected area electron diffraction (SAED) pattern of the sample appeared as the combinatorial of both the components with majority diffractions generated from ZnO however, some minor reflections originated from Mn_3O_4 are also observable. The HRTEM images (Fig. 7c and d) focusing the junction point of the components of the composite revealed two discrete fringe patterns with the spacing of 0.29 nm and 0.38 nm that corresponded to cubic Mn_3O_4 and wurtzite ZnO with hexagonal geometry [35–37].

The comparison of the charge retention ability of the pure and Mn_3O_4 loaded ZnO composites, in the dark and under illumination, is shown in Fig. 8a and b. In the dark, under the influence of external biasing, 0.5%Mn_3O_4-ZnO, exhibited a better charge retention ability as compared to pure ZnO and other Mn_3O_4 loaded catalysts. The surface induced defects by the lower concentration on Mn_3O_4 are the probable cause of the effect. A drastic change in the charge retention ability of the composites was noticed under illumination. The charging time for 1%, 3% and 5%Mn_3O_4 loaded ZnO catalysts was reduced as compared to pure, 0.5% and 10%Mn_3O_4 loaded ZnO composites, whereas a significant change in the discharge time was observed that demonstrated their ability to retain the charge with the transfer of the photogenerated holes from the valence band of ZnO to that of Mn_3O_4.

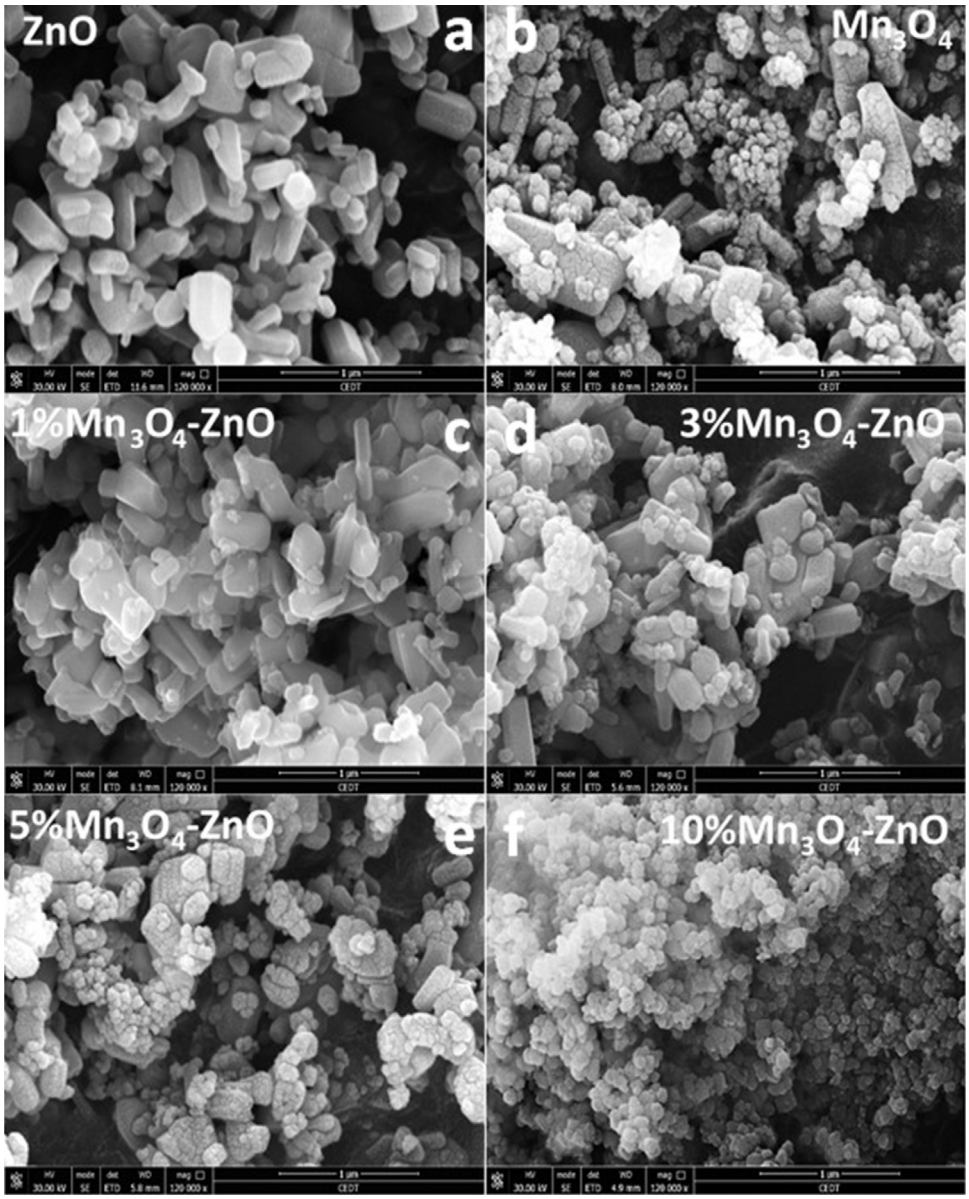

Fig. 6. The comparison of FESEM images of (a) bare ZnO, (b) pure Mn_3O_4 and (c-f) Mn_3O_4 loaded ZnO composites at high resolution (120,000×).

The electrochemical impedance spectroscopy (EIS) is regarded as a vital tool for the approximation of the charge transport in the materials [38,39]. In the current study, the EIS spectra of Mn_3O_4 loaded ZnO composites were recorded in the dark and under illumination to estimate the effect of Mn_3O_4 on the charge transport properties of ZnO. It is important to mention here that in the dark, the charge transfer is governed purely by the externally applied potential whereas under illumination the same is incremented by the photogenerated excitons under illumination. The comparison of both may lead to better assessment of the decrease in the charge transfer resistance. The EIS Nyquist plots of pure ZnO and the composites in the dark and under illumination are presented in Fig. 8c and d. Under dark conditions, compared to pure ZnO, the composite formation resulted in the reduced radius of the semicircular portion that depicted the decreased resistance to the electron transfer (Fig. 8c). Except for 10% Mn_3O_4 loaded ZnO composite, a similar behavior with minor variations was observable. Compared to pure ZnO, a significant variation in both low (linear) and high frequency (semicircular region) was noticed. Contrary to the situation in the dark where 0.5%Mn_3O_4 loaded ZnO offered the minimum resistance to the electron transfer, 3% Mn_3O_4 loaded ZnO emerged as the catalyst in illumination (Fig. 8d) with lowest charge transfer resistance based on the least diameter of the semicircular region and maximum increase in the high-frequency area [33]. The charge transfer resistance of the other composites was higher than 1% Mn_3O_4 loaded catalysts whereas the resistance of 10% composite was comparable to 0.5% Mn_3O_4 loaded ZnO composite. With the results presented above, it might be inferred that 1%Mn_3O_4 loading is probably an adequate surface concertation for optimum charge transfer that may result in the better photocatalytic activity as compared to other composites and pure ZnO.

As the current study was designed to enhance the photocatalytic activity of ZnO, the photocatalytic performance of bare ZnO and Mn_3O_4-ZnO heterostructures was evaluated for the removal (degradation/mineralization) of 4-bromophenol (4-BP) and 4-chlorophenol (4-CP) in the exposure of complete spectrum natural sunlight. The choice of the model pollutant was based on their stability in the aqueous solution due to the intermolecular attractive forces, inductive and resonance effects. Prior to exposure, the suspensions were kept in the dark for an hour to establish

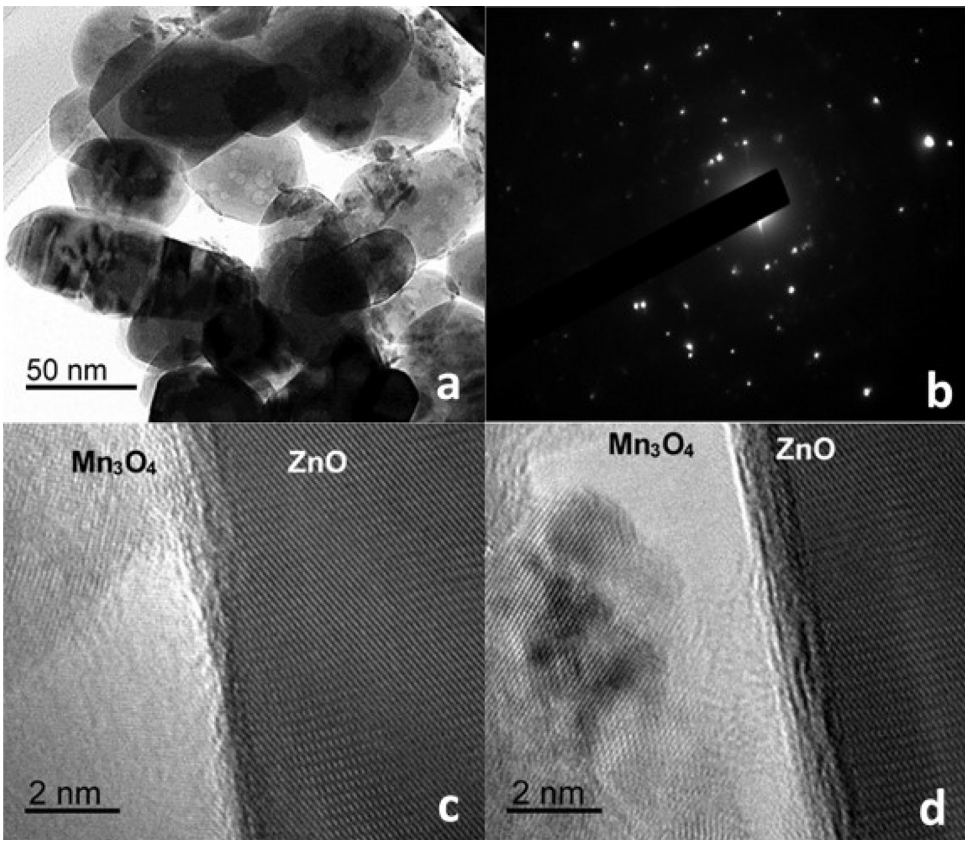

Fig. 7. The typical (a) TEM image (b) the SAED pattern of 3% Mn_3O_4 loaded ZnO composite whereas (c) and (d) shows the fringe patterns of the same.

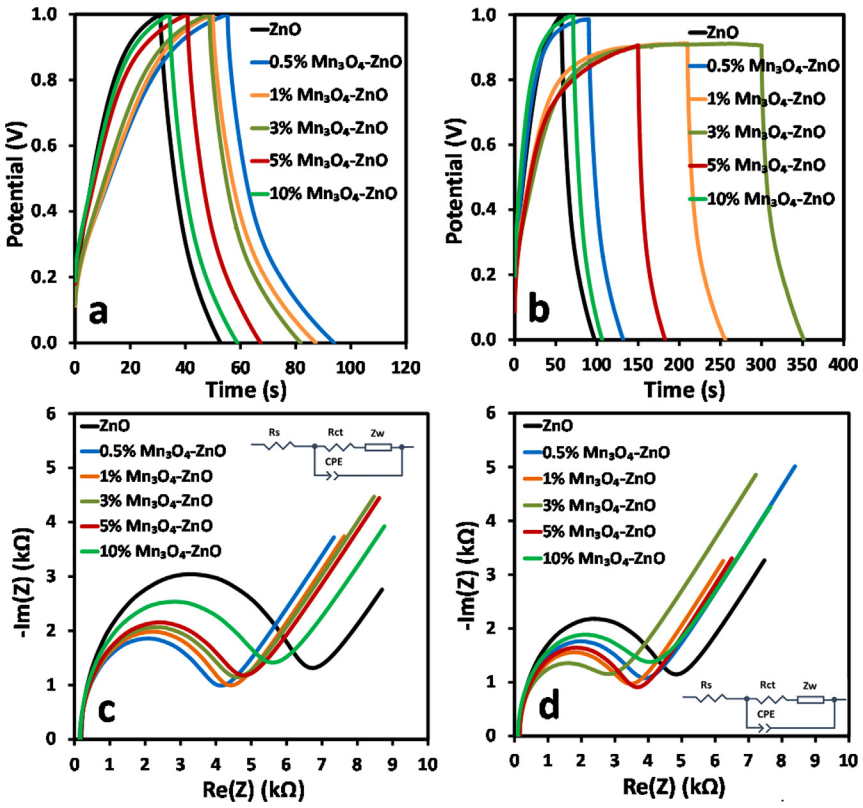

Fig. 8. The comparison the charge-discharge curves (a, b) and EIS response (c, d) of pure ZnO and Mn_3O_4 loaded ZnO composites in dark and under illumination, respectively.

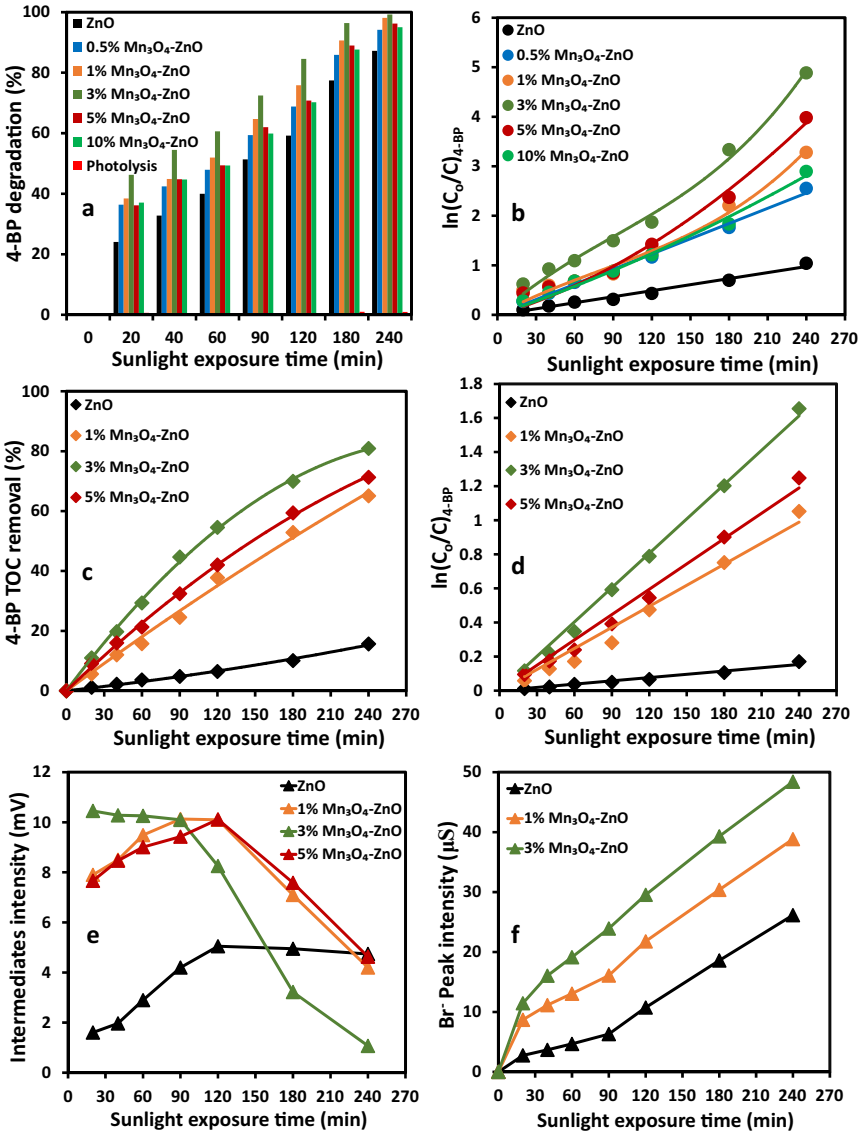

Fig. 9. The comparison of (a) degradation (b) rate of removal (c) TOC removal (d) C/C_o (e) major intermediate removal and (d) released Br^- ions in the removal of 50 ppm 4-bromophenol under sunlight exposure over pristine ZnO, 1%, 5% and 10% Mn_3O_4 loaded ZnO composites.

the catalyst-substrate equilibrium and simultaneous evaluation of the magnitude of adsorption of the substrates. Interestingly, the adsorption of 4-BP on pure ZnO and Mn_3O_4 loaded composites was in the range of 12.5–14% of the actual concentration (50 ppm). No noticeable change in the adsorption of 4-BP on ZnO was observed with the loading of Mn_3O_4. The comparison of the actual HPLC chromatograms as a function of sunlight exposure time for all the catalysts is shown in Fig. S1 (Supplementary material). Instead of measuring the actual concentration of the substrate, the decrease in the peak intensity, being complementary to concentration, was selected as an estimate for the removal of 4-BP. The comparison of the percentage removal of 4-BP with the increasing sunlight exposure time is presented in Fig. 9a. In the initial 20 min of sunlight exposure, ~24%, ~39% and ~46% of 4-BP was removed by 1% and 3% and 3% Mn_3O_4 loaded ZnO composites whereas ~9.5%, ~36%, and ~24% removal was measured over pure ZnO, 0.5%, and 10% Mn_3O_4 loaded ZnO catalysts. An increasing trend in the removal of the substrate was noticed with the increasing Mn_3O_4 loading till 3% followed by a decrease afterward. Although ~85% of 4-BP was removed in 120 min, however, the complete removal (≥99.5) was witnessed in 240 min of sunlight exposure over 3% Mn_3O_4 modified ZnO whereas ~65% degradation was observed for pure ZnO in the same period. This significantly lower degradation of 4-BP substrate by ZnO as compared to Mn_3O_4 modified ZnO catalysts was attributed to low harvesting of excitons especially electrons to the dissolved/adsorbed oxygen to generate reactive oxygen species (ROS). For the as-synthesized catalysts, the kinetics of removal of 4-BP was estimated by applying the Langmuir-Hinshelwood kinetic model for pseudo-first order reactions. The comparison of the plots of $\ln(C_o/C)$ versus the sunlight exposure time (t) of the synthesized catalysts and that of pure ZnO is shown in Fig. 9b. A deviation from the kinetic model was witnessed for the catalysts with higher activity i.e. 1%, 3% and 5% Mn_3O_4-ZnO composites whereas, the rate of removal was linear for pure, 0.5% and 10% Mn_3O_4 loaded ZnO composites i.e. the catalysts with low and moderate activity. Interestingly, for the catalysts with relatively high activity, the rate of removal was linear in the initial 120 min of exposure, however, increased abruptly with the decreasing concentration of the substrate. Based on the above-mentioned observations, it might be inferred that the L-H kinetic model holds well for the catalysts with moderate or lower activity whereas violated for the catalysts with high activity that was consistent with our previously

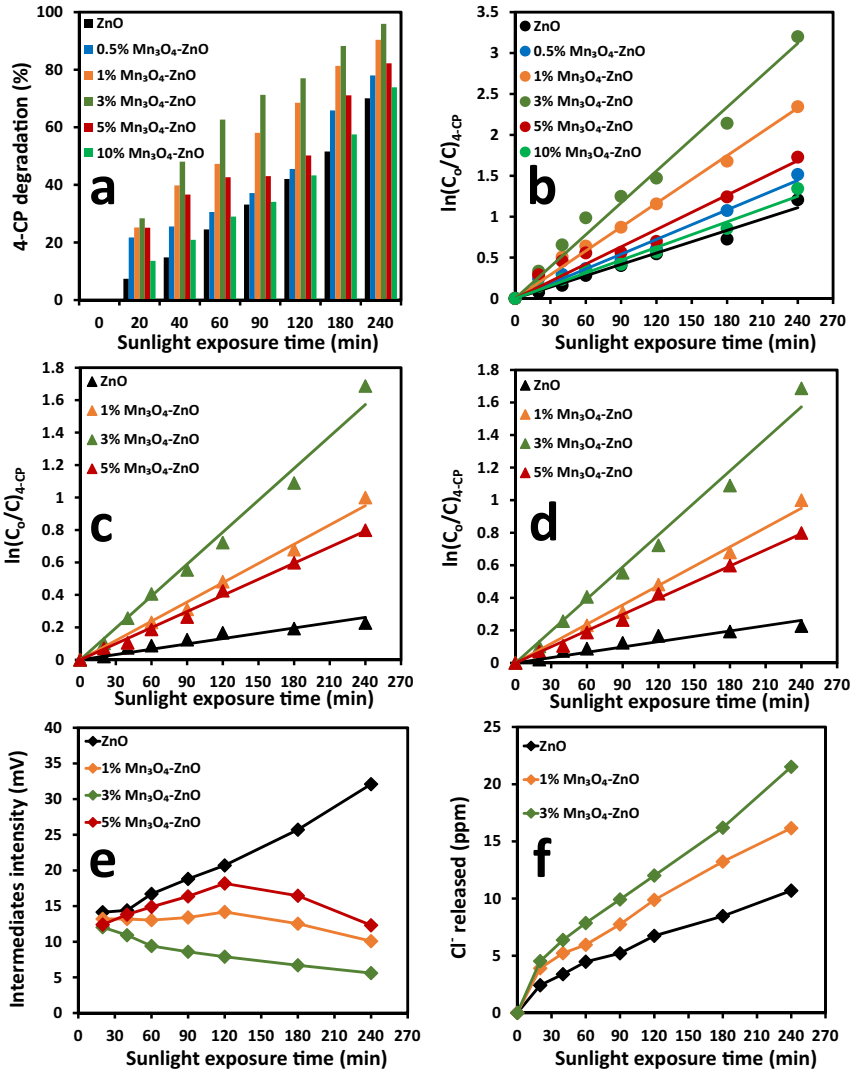

Fig. 10. The comparison of (a) degradation (b) rate of removal (c) TOC removal (d) C/C_o (e) major intermediate removal and (d) released Cl^- ions in the removal of 50 ppm 4-chlorophenol under sunlight exposure over pristine ZnO, 1%, 5% and 10% Mn_3O_4 loaded ZnO composites.

reported observations [31,32]. The monitoring of the changes in the total organic carbon (TOC) during photocatalytic removal processes is equally important to assess the complete elimination of substrates efficiently. For clarity, instead of all the catalysts, the comparison of TOC removal (mineralization) of 4-BP in the complete spectrum of sunlight illumination over bare ZnO, 1%, 3% and 5% Mn_3O_4 modified ZnO is presented in Fig. 9c. The synthesized composites showed significantly enhanced mineralization of 4-BP substrate as compared to bare ZnO. Compared to ~15% mineralization of 4-BP over pure ZnO in 4 h of sunlight exposure, the 1%, 3%, and 5% Mn_3O_4-ZnO removed ~69%, ~81% and ~75% of TOC respectively in the same period. The 3% Mn_3O_4-ZnO composite reduced ~20.58 ppm of TOC in 50 ppm of 4-BP to 3.98 in 240 min of exposure whereas ZnO was able to reduce the same to 17.56 ppm in the same exposure time that indicated an increase of 4.5 times in the mineralization ability of ZnO after loading 3% of Mn_3O_4. The graphical evaluation of the rate of TOC removal is presented in Fig. 9d. For the mineralization process, the L-H kinetic was validated with the acceptable correlation. The reasonably lower rates of mineralization as compared to that of degradation clearly reflected the multistep nature of the mineralization. Additionally, the rapid removal of the substrates also proposes the ease in the degradation as compared to mineralization that can be accomplished by any minor structural change. Therefore, the degradation does not essentially mean the complete removal of the substrate rather referred to as transformation into another compound. In the HPLC profiles (Fig. S1; Supplementary material) the appearance of additional peaks revealed the formation of intermediates during the degradation process that depicted the multi-step nature of the removal process. Fig. 9e shows the variations in the concentration of the major intermediate observed at the retention time of ~1.91 min for pure ZnO and 1%, 3% and 5% Mn_3O_4-ZnO composites during the degradation of 2-BP in sunlight exposure. A mild increase in the peak intensity of the above-mentioned intermediate followed by a sharp decrease was witnessed with the increase in the exposure time for 3% Mn_3O_4-ZnO composite whereas a gradual increase up to 180 min of exposure followed by a decrease in the final hour was observed for 1% and 5% Mn_3O_4-ZnO composites. Contrary to Mn_3O_4 modified ZnO catalysts, an increasing trend in the concentration of the intermediate was observable for pure ZnO with sunlight exposure time. The situation referred to the priority interaction of ROS with the 4-BP substrate, the formation of intermediates and further interaction of intermediates with ROS to smaller fragments. The growth and decay of the low or moderate intensity peaks in the HPLC chromatograms (Fig. S1; Supplementary material) verified the same. The catalysts with the maximum

ability of charge transfer to the absorbed species for the generation of ROS exhibit the optimum simultaneous activity for the removal of the actual substrate as well as the intermediates. Therefore, it might be deduced that the population of ROS or the ability of catalysts to generate ROS is the key controlling factor in the degradation process. In the aqueous phase photocatalytic process, along with the number of ROS generated, the hydroxyl ($HO^{\bullet}$) and superoxide anion ($O_2^{\bullet-}$) radicals are regarded as the primary oxidants. Keeping in view the chemically different nature of both, to assess the probable role of each in the oxidation process the ions released during the degradation process were monitored with the view that the interaction of $O_2^{\bullet-}$ being negatively charged in nature may lead to the release of ample ions in the system whereas fewer ions may be observed as a result of the interaction of $HO^{\bullet}$. The comparison of the released Br^- ions over pure ZnO 1% and 3% Mn3O4-ZnO composites is presented in Fig. 9f whereas the typical IC profile of the Br^- ions released during the degradation of 4-BP over 3% Mn_3O_4-ZnO is presented in Fig. S2a (Supplementary material). The release of ample Br^- ions consistent with the degradation of 4-BP perceptibly indicated the major role of charged ROS ($O_2^{\bullet-}$ radicals) instead of the neutral oxidant such as hydroxyl ($HO^{\bullet}$) radicals. The further transformation of Br- ions, either by the interaction of ROS or the excitons, to BrO3- ions is also observable on the IC profile.

The comparison of the HPLC chromatograms of all the catalysts is presented in Fig. S3 (Supplementary material), where the decrease of the varying magnitude in the concentration of 4-CP and the ample formation of intermediates in sunlight exposure is observable. The comparison of the percentage degradation of 4-CP, calculated from the peak height of 4-CP in HPLC profiles, as a function of sunlight irradiation is shown in Fig. 10a. A trend similar to that of 4-BP was noticed in the removal of 4-CP as well. In the initial 60 min of sunlight exposure, ~62% of 4-CP was removed over 3% Mn_3O_4-ZnO composite whereas ~24%, ~30%, ~47% and ~23% of the substrate was removed over pure ZnO, 0.5%, 1%, 5% and 10% Mn_3O_4 loaded catalysts. After 240 min of sunlight exposure among all modified ZnO composites, a maximum degradation of ~95% was noticed for 3% Mn_3O_4 loaded ZnO whereas in the pure ZnO degraded ~70% of the pollutant in the same period. The validity of the Langmuir-Hinshelwood (L-H) kinetic model was evaluated by plotting $\ln(C_o/C)$ versus the exposure time (t). As presented in Fig. 10b, the L-H kinetic model was validated with acceptable correlation in the removal of 4-CP. The evaluated rate constants were 0.0053 min^{-1}, 0.0065 min^{-1}, 0.0097 min^{-1}, 0.0133 min^{-1}, 0.0076 min^{-1} and 0.0050 min^{-1} for pure ZnO, 0.5%, 1%, 3%, 5% and 10% Mn_3O_4-ZnO composites respectively. The ~2.6 times higher degradation rate of 4-CP over 3% Mn_3O_4-ZnO (0.0133 min^{-1}) as compared to pure ZnO (0.0053 min^{-1}) may be attributed to Mn_3O_4 mediated enhanced generation of ROS by trapping the excitons prior to recombination. Fig. 10c shows the comparison of TOC removal (mineralization) of 4-CP in the complete spectrum of sunlight exposure over bare ZnO, 1%, 3% and 5% Mn_3O_4 modified ZnO. In 120 min of exposure, ~78% of the substrate was degraded whereas a mineralization of ~55% was observed for 3% Mn_3O_4-ZnO composite. A similar trend was witnessed for all the catalysts that indicated the priority engagement of ROS in the degradation process rather than TOC removal. After 240 min of sunlight exposure, the observed mineralization observed over ZnO, 1%, 3%, and 5% Mn_3O_4 composites was ~20%, ~63%, ~81% and ~55% respectively. Moreover, the 3% Mn_3O_4 loaded ZnO composite reduced the initial TOC contents of ~20.86 ppm to ~5.18 in 240 min of exposure whereas ZnO was able to reduce TOC content up to ~14.33 ppm in same exposure time, that indicated ~2.8 times enhancement in the mineralization. The graphical evaluation of the rate constants of the mineralization of 4-CP over pure, 1%, 3% and 5% Mn_3O_4-ZnO composites in sunlight exposure is presented in Fig. 10d. The higher ability to oxidize organic contents with significantly higher rate constant was noticed for 3% Mn_3O_4 loaded composite. The evaluated rate constants for pure ZnO, 1%, 3% and 5% Mn_3O_4-ZnO composites were 0.0009 min^{-1}, 0.0039 min^{-1}, 0.0030 min^{-1} and 0.0067 min^{-1}, respectively, that were significantly lower than the degradation process, however, comparable with the mineralization of 4-BP. Similar to 4-BP degradation, the major intermediate in the degradation of 4-CP also appeared at the retention time of ~1.9 mins (Fig. 10e) and an increase in the concentration of intermediate was noticed with the increasing exposure time for pure ZnO whereas a decrease was noticeable that predicted the better mineralization ability of the 3% Mn_3O_4-ZnO composite as compared to pure ZnO. The pattern of the release of Cl^- ions was consistent with the degradation of 4-CP over pure ZnO, 1% and 3% Mn_3O_4-ZnO composite (Fig. 10f). As presented in Fig. S2b (Supplementary material), the typical IC profile for the release of Cl- ions during the degradation of 4-CP over 3% Mn_3O_4-ZnO composite in sunlight exposure, the identification of ClO_3^- ions in the IC profiles, the further interaction of Cl^- with the ROS or excitons was also anticipated.

With the appearance of some recent publication contradicting the generation, survival and the plausible role of hydroxyl radicals in the photocatalytic removal process has turned into a conflicting issue as the majority of the publication designate hydroxyl radicals as the key rather sole contributors in the degradation process [40,41]. Additionally, the studies support the minor or null involvement of hydroxyl radicals in the degradation process and label superoxide anion radicals as the majority contributors [42,43] as the mobility, diffusion and the reactivity of the superoxide anion ($O_2^{\bullet-}$) radicals in the bulk solution is also well established [44]. Besides other minor factors, as per our perception, the knowledge of the edge potentials of semiconductor/s involved can furnish vital clues regarding the proportional generation of ROS (either superoxide anion or hydroxyl radicals). Another salient feature of

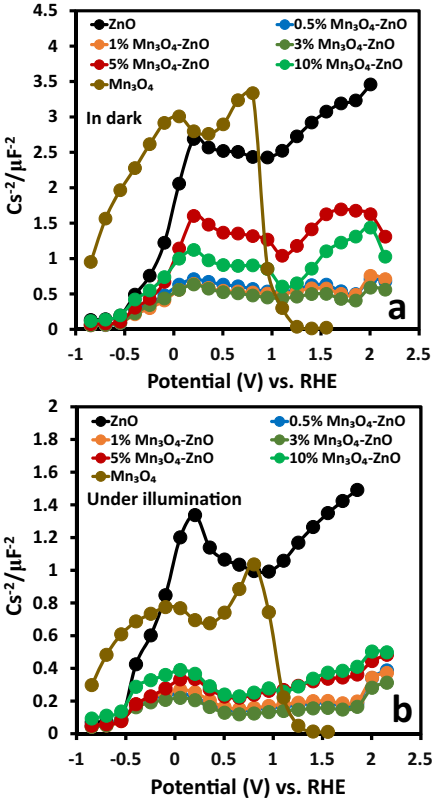

Fig. 11. The comparison of the Mott-Schottky plots of pure ZnO, Mn_3O_4 and Mn_3O_4 loaded ZnO composites (a) in dark and (b) under illumination.

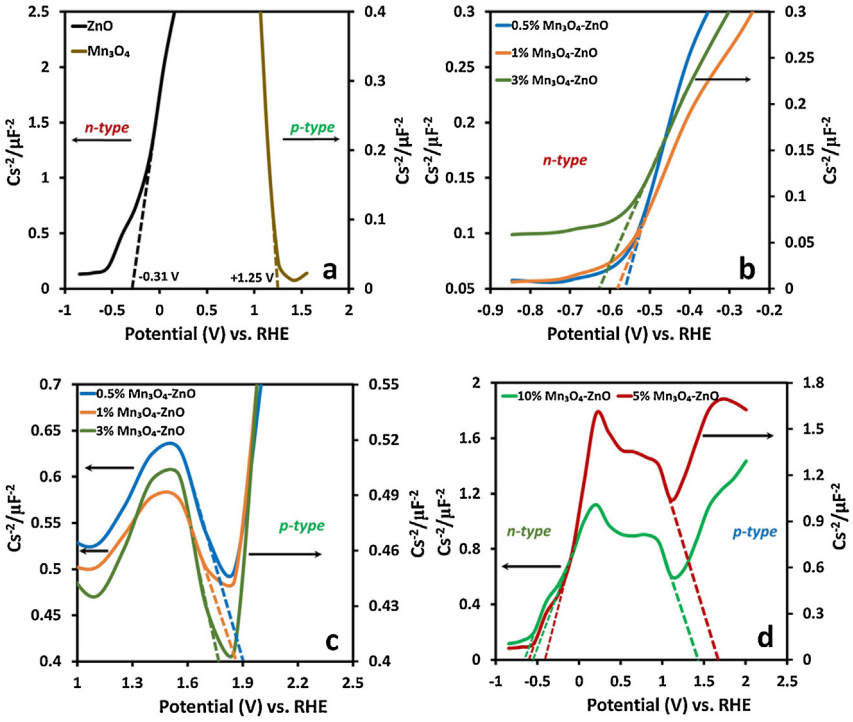

Fig. 12. The graphical evaluation of the flatband potential of pure ZnO, Mn_3O_4 and Mn_3O_4 loaded ZnO composites.

assessing the band edge potentials, when dealing with the composite photocatalysts, is the understanding of the trapping of the excitons generated in the "host", with the absorption of photons, by the "guest" component to avoid recombination. In the current study, the probable modes of charge transfer and the probable formation of superoxide anion or hydroxyl radicals was investigated by measuring the flat-band (V_{fb}) potentials of pure Mn_3O_4, ZnO, and synthesized composites by staircase potential electrochemical impedance spectroscopy (SPEIS). The Mott-Schottky plots of the SPEIS analysis ($Cs^{-2}/\mu F^{-2}$ versus the applied potential (V)) of pure Mn_3O_4, pure ZnO, and the synthesized composites in the dark and under illumination are presented in Fig. 11a and b, where the characteristic onsets in the negative and positive potential regions for pure ZnO and Mn_3O_4 authenticated the *n-type* and *p-type* nature of both the materials, respectively. In the dark measurements, the appearance of dual onsets, both in the negative and positive potential region, characteristic of *p-n* junction materials specified the existence of both the characters in the composites [45]. The curves indicated the dominance of the n-type character at the lower Mn_3O_4 loadings up to 3% whereas the *p-type* character was enhanced at higher loadings. Under illumination, the decreased intensity specified the improved charge transfer in the composites. Additionally, the depletion of *p-type* character and the dominant *n-type* features were noticed for all the composites. The extrapolation of the linear portion of the curves in the negative or positive potential region or both (for composites) to the x-axis resulted in the V_{fb} of the respective material. The graphical evaluation of V_{fb} for pure ZnO and Mn_3O_4 are presented in Fig. 12a. The evaluated V_{fb} values of −0.31 V and +1.25 V for ZnO and Mn_3O_4, respectively, were in close agreement with the literature values. As the V_{fb} of a *p-type* semiconductor is considered as the potential of the valence band and that of n-type as conduction band [46], the evaluated conduction and valence band edges, using the bandgap energies of 3.2 eV and 2.5 eV as estimated from DRS analysis (Fig. 2), were −0.31 V (CB), +2.89 V (VB) and −1.25 V, +1.25 V for ZnO and Mn_3O_4, respectively. The close match of the evaluated values with that of literature established the efficacy of the adopted procedure for the accurate experimental measurement of the potential of band edges [47]. The evaluated values of V_{fb} for the *n-type* portion of the 0.5%, 1% and 3% were −0.55 V, −0.57 V and −0.64 V, respectively (Fig. 12b), whereas for the *p-type* component were observed at +1.7 to +1.9 V (Fig. 12c). As presented in Fig. 12d, the enhancement in the p-type character was witnessed with the increasing loading of Mn_3O_4 as the positive potentials were shifted to further lower values of +1.68 V and +1.42 V for 5% and 10% Mn_3O_4 loaded composites. Similarly, a decrease in the onset values in the negative potential region was observed. The calculations based on the measured V_{fb} verified the sufficiently negative conduction band edges for the reduction of adsorbed/dissolved oxygen that requires −0.28 V. On the other hand, although in the permissible limits, the decreased potential of the composites, for water oxidation, predicted the low yield of hydroxyl radicals. Besides the suitability of the band edges of the individual components of the composites for the generation of ROS, the compatibility of the band edges for the optimal synergic mutual charge transfer is also an essential parameter for the enhanced generation of ROS. Additionally, the fraction of the photons absorbed by the active component (ZnO in the current case) and the surface coverage by the minor component (Mn_3O_4) also contribute in this regard. Furthermore, based on the measured band edge potentials for pure ZnO (−0.31 V, +2.89 V) and Mn_3O_4 (−1.25 V, +1.25 V), with the optimum probability of the transfer of photogenerated h^+ from the conduction band of ZnO to that of Mn_3O_4, it might be predicted that the prime charge separation is achievable with the generation of excitons by ZnO. A brief account of the probable charge transfer transitions as a function of the Mn_3O_4 loading, in the exposure of complete spectrum sunlight, is summarized in Scheme 1.

From the discussion of outcomes on the PL, electrochemical characterization and photocatalytic removal of both the substrates (4-BP and 4-CP), it might be inferred that although the surface Mn_3O_4 entities serve as the effective suppressors for the exciton recombination process, however, the optimization of the surface loading of the modifier (Mn_3O_4 in the current case) is essential for the maximum efficacy. The enhanced removal efficiency of 3%

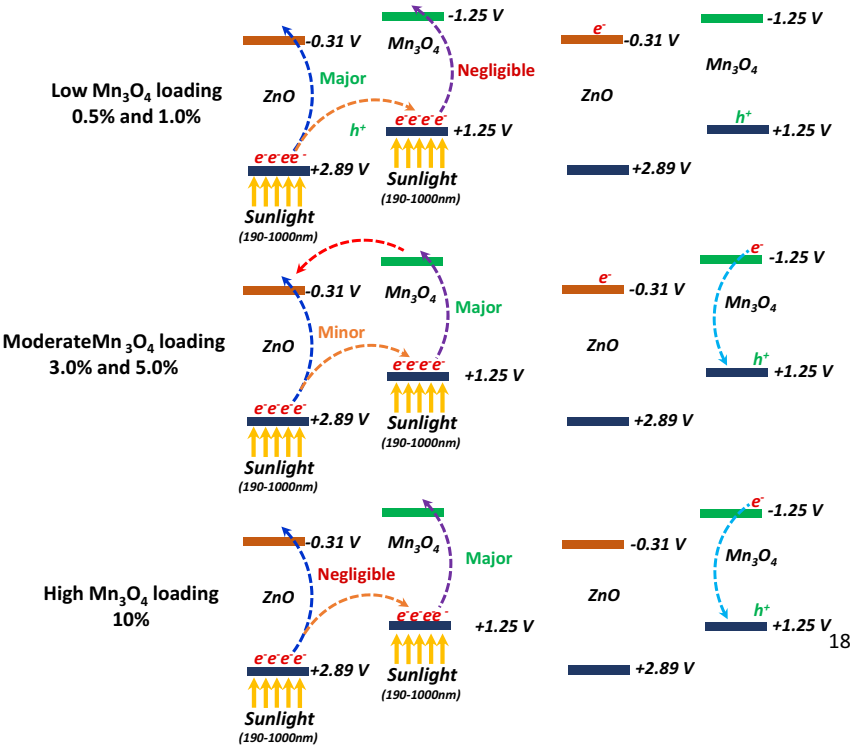

Scheme 1. The probable major and minor transitions in Mn_3O_4-ZnO composites as a function of increasing Mn_3O_4 loading.

Mn_3O_4-ZnO composite is suggestive of the existence of optimal charge trapping and transport synergy between the components of the composite that leads to the enhanced generation of ROS rather than being squandered in the recombination process. Probably, the low concentration of Mn_3O_4 leads to the higher rate of recombination process that results in the comparatively lower activity of 0.5% and 1% Mn_3O_4-ZnO composites. It can also be speculated that in 0.5%, 1%, and 3% composites the majority of the incident photons are absorbed by the ZnO rather than a Mn_3O_4 modifier. The reduced absorption of photons by ZnO due the direct absorption of a significant fraction of incident photons by the Mn_3O_4 component results in the lower activity of 5% Mn_3O_4-ZnO composite. For 10% Mn_3O_4-ZnO composite, due to higher surface coverage, the situation is further aggravated, as the major portion of the incident photons is absorbed by the Mn_3O_4 that leads to further decrease in the activity.

In the current study, the favorable potentials of the conduction band edges of both ZnO and Mn_3O_4, the rapid degradation, the release of Cl^- and Br^- ions corresponding to degradation and significantly high TOC removal support the major involvement of superoxide anion ($O_2^{\bullet-}$) radicals in the degradation process. Concurrently, in the presence of the suitable valence edge potentials for water oxidation, the existence of the hydroxyl ($HO^{\bullet}$) radicals in the system cannot be completely negated, therefore, may be regarded as minor contributors. The intensity of the released Cl^- and Br^- ions coherent with the degradation process also spot the carbon atom at 4-position as the probable interaction site for the incoming $O_2^{\bullet-}$ radicals due to the induction of partial positive charge by the electronegative group therefore, it might be deduced that the degradation process proceeds with the displacement of halogen ions with $O_2^{\bullet-}$. The identification of mostly oxygenates in the GC–MS analysis (Fig. S4b; Supplementary material) of the sample drawn after 60 min of sunlight exposure for 3% Mn_3O_4-ZnO composite verified not only the cleavage of the aromatic ring but also the insertion of the oxygen in the carbon chain leading to the formation of another stream of polar compounds that are further interacted by the $O_2^{\bullet-}$ radicals until complete mineralization. The pictorial presentation of the plausible mechanism of degradation and mineralization is presented in Scheme 2.

Another objective of the study was to evaluate the effect of nature of the substituents on the degradation/mineralization process. The higher rate of degradation of 4-BP than that of 4-CP reflected the better stability of 4-CP against the ROS attack. Probably, the higher electronegativity of Cl as compared to Br group impart additional stability to C—Cl bond as compared C—Br bond. The amplified magnitude of the intramolecular hydrogen bonding further augments the stability to 4-CP. On the other hand, the relatively low electronegativity and larger size (0.94 A) of Br as compared to Cl (0.79 A) group make it more labile and susceptible to ROS attack. The lower pace of degradation of 4-CP also affected the process of mineralization as well. The proportional relationship between the two processes again depicts the primacy of the ROS for the substrate. To verify the assumption further, the comparison of the HPLC and GC–MS chromatograms of both 4-BP and were plotted and presented in Fig. S4a and b (Supplementary material), respectively. The formation of indistinguishable products as intermediates indicated that both the substrates are not only degraded by the interaction of identical ROS but also proceed through the identical mechanism. The decay and growth the peaks indicate the further interaction of ROS leading to the formation of smaller fragments that are mineralized finally. Additionally, an escalation in the mineralization was observed with the depleting concentration of the substrates.

It is well-established fact that ZnO undergoes dissolution under illumination [48]. The process of photo-corrosion of ZnO under illumination is described by the set of Eq. (1)–(3) given below.

$$ZnO + h\nu \overset{h\nu \geq Eg}{\rightarrow} ZnO\left(h_{vb}^{+} + e_{cb}^{-}\right) \quad (1)$$

$$ZnO + 2h_{vb}^{+} + H_2O \rightarrow Zn^{2+}(\text{solution}) + \frac{1}{2}O_2(\text{solution}) \quad (2)$$

$$ZnO + 2e_{cb}^{-} \rightarrow Zn^{2+}(\text{solution}) + 2O^{-}(\text{surface}) \quad (3)$$

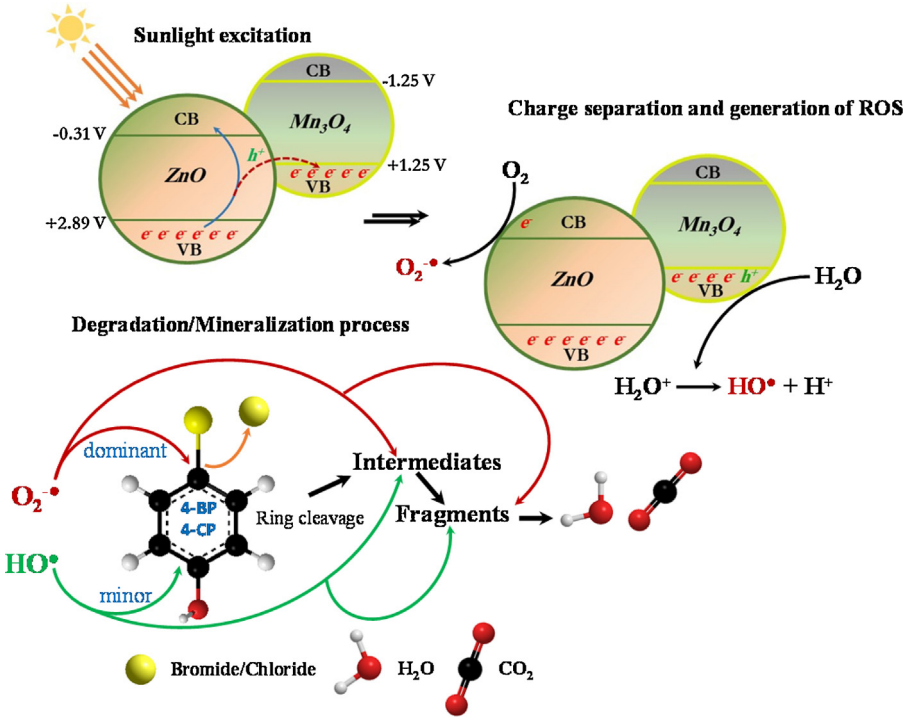

Scheme 2. The plausible route of removal for 4-BP and 4-CP over 1% Mn_3O_4-ZnO composite in sunlight exposure.

The comparison of the CVs of the pure ZnO and the synthesized catalysts, in the dark and under illumination, is given in Fig. S5a and b (Supplementary material). The hexagonal ZnO showed a stable response in dark and the redox couple at −1.18 V and −1.36 V corresponded to the formation of zincate ions, $(Zn(OH)_4^{2-})$, under the influence of applied potential. Though with the decreased peak intensity, the same set of redox peaks was noticed for the composites. The measurements under illumination revealed the appearance of an additional peak at ∼−0.93 V due to the release of Zn^{2+} ions in the solution (Fig. S5b). The same was completely suppressed (featureless) for the Mn_3O_4-ZnO composites that depicted the supporting role of surface Mn_3O_4 for elimination the probable causes of photo-corrosion. Based on the experimentally evaluated potentials of the valence band edges, it might be predicted that the principal energetically favored transition, with the absorption of photons by the ZnO, is the transfer of positive entities (h^+) produced as a result of bandgap excitation, from the valence band of ZnO to that of Mn_3O_4 (Scheme 1). It can also be speculated that the phenomenon of photo-corrosion occurs due to the self-oxidation of ZnO by the photogenerated holes (Eq. (2)). In composites, the mutual charge transfer between components (from ZnO to Mn_3O_4) results in the non-availability of the h^+ for the oxidation thus the release of Zn^{2+} is dramatically reduced (Scheme 1).

4. Conclusions

Composite formation by loading the surface of hexagonal ZnO with that of Mn_3O_4 has proved to be a vital option not only for enhancing the photocatalytic activity in the natural sunlight exposure but also protecting its surface against photocorrossion. The optimum loading of the modifier is the vital factor for the foremost charge trapping and transfer process. The decrease in the emission intensity in the PL analysis provides only a rough estimation of the ability of the modifier to suppress the exciton recombination process, however, does not guarantee the optimum activity with the decreased emission intensity. The correlation between the predicted photocatalytic activity by electrochemical tools and the results of the actual photocatalytic experiments proved the efficacy of the adopted procedure. The information extracted from the electrochemical analysis of the composites revealed better insight of the charge trapping and transfer as compared to PL spectroscopy. In the photocatalytic experiments, the experimental evidence revealed:

- Superoxide anion $(O_2^{\bullet-})$ radicals as the major participants in the removal process.
- Better stability of 4-CP as compared to 4-BP.
- Cl^- and Br^- serves as facilitators in the degradation process.
- Similar intermediates in the degradation of both the substrates.
- Priority interaction of ROS with the substrates rather than intermediates.
- Multistep nature of the mineralization process.
- Further interaction of ROS with larger intermediates to smaller fragments till complete mineralization.
- Evidence of the further interaction of released ions with the ROS or excitons.

Acknowledgements

A. Hameed, M. Aslam, M.T. Qamar, and Iqbal M.I. Ismail are thankful to Center of Excellence in Environmental Studies (CEES), King Abdulaziz University and Ministry of Higher Education (MoHE), KSA, for support. M.T. Qamar also gratefully acknowledge the support from Chemistry Department, Faculty of Science, King Abdulaziz University.

Appendix A. Supplementary data

Supplementary data associated with this article can be found, in the online version, at http://dx.doi.org/10.1016/j.apcatb.2016.08.004.

References

[1] A. Hameed, M. Aslam, I.M.I. Ismail, S. Chandrasekaran, M.W. Kadi, M.A. Gondal, Appl. Catal. B: Environ. 160–161 (2014) 227–239.
[2] M. Aslam, I.M.I. Ismail, S. Chandrasekaran, T. Almeelbi, A. Hameed, RSC Adv. 4 (2014) 49347–49359.
[3] S. Rehman, R. Ullah, A.M. Butt, N.D. Gohar, J. Hazard. Mater. 170 (2009) 560–569.
[4] M.E. Manríıquez, T. Líopez, R. Gíomez, J. Navarrete, J. Mol. Catal. A: Chem. 220 (2004) 229–237.
[5] M. Aslam, I.M.I. Ismail, T. Almeelbi, S. Chandrasekaran, A. Hameed, Chemosphere 117C (2014) 115–123.
[6] I.M.I. Ismail, M. Aslam, T. Almeelbi, S. Chandrasekaran, A. Hameed, RSC Adv. 4 (2014) 16043–16046.
[7] S.G. Kumar, K.S.R. Koteswara Rao, RSC Adv. 5 (2015) 3306–3351.
[8] A. Hameed, T. Montini, V. Gombac, P. Fornasiero, J. Am. Chem. Soc. 130 (2009) 9658–9659.
[9] A. Hameed, T. Montini, V. Gombac, L. Felisari, P. Fornasiero, Chem. Phys. Lett. 483 (2009) 254–261.
[10] Z. Zhang, C. Shao, X. Li, L. Zhang, H. Xue, C. Wang, Y. Liu, J. Phys. Chem. C 114 (2010) 7920–7925.
[11] R. Saravanan, S. Karthikeyan, V.K. Gupta, G. Sekaran, V. Narayanan, A. Stephen, Mater. Sci. Eng. C 33 (2013) 91–98.
[12] J. Wang, T. Tsuzuki, B. Tang, X. Hou, L. Sun, X. Wang, ACS Appl. Mater. Interfaces 4 (2012) 3084–3090.
[13] A. Hameed, T. Montini, V. Gombac, P. Fornasiero, Photochem. Photobiol. Sci. 8 (2009) 677–682.
[14] D. Chen, A.K. Ray, Appl. Catal. B Environ. 23 (1999) 143–157.
[15] S.-H. Wu, J.-L. Wu, S.-Y. Jia, Q.-W. Chang, H.-T. Ren, Y. Liu, Appl. Surf. Sci. 287 (2013) 389–396.
[16] B. Zhou, X. Zhao, H. Liu, J. Qu, C.P. Huang, Sep. Purif. Technol. 77 (2011) 275–282.
[17] M.A. Oturan, J.J. Aaron, Crit. Rev. Environ. Sci. Technol. 44 (2014) 2577–2641.
[18] C.-C. Wang, J.-R. Li, X.-L. Lv, Y.-Q. Zhang, G. Guo, Energy Environ. Sci. 7 (2014) 2831–2867.
[19] M. Aslam, I.M.I. Ismail, N. Salah, S. Chandrasekaran, M.T. Qamar, A. Hameed, J. Hazard. Mater. 286 (2015) 127–135.
[20] M.N. Chong, B. Jin, C.W.K. Chow, C. Saint, Water Res. 44 (2010) 2997–3027.
[21] S. Banerjee, D.D. Dionysiou, S.C. Pillai, Appl. Catal. B Environ. 176 (2015) 396–428.
[22] N.C.S. Selvam, S. Narayanan, L.J. Kennedy, J.J. Vijaya, J. Environ. Sci. 25 (2013) 2157–2167.
[23] M. Aslam, I.M.I. Ismail, S. Chandrasekaran, A. Hameed, J. Hazard. Mater. 276 (2014) 120–128.
[24] D.S. Bhatkhande, V.G. Pangarkar, A.A.C.M. Beenackers, J. Chem. Technol. Biotechnol. 77 (2002) 102–116.
[25] R. Saravanan, V.K. Gupta, V. Narayanan, A. Stephen, J. Taiwan Inst. Chem. Eng. 45 (2014) 1910–1917.
[26] T. Yamashita, A. Vannice, Appl. Catal. B Environ. 13 (1997) 141–155.
[27] T.K. Ghorai, S. Pramanik, P. Pramanik, Appl. Surf. Sci. 255 (2009) 9026–9031.
[28] B. Han, F. Zhang, Z. Feng, S. Liu, S. Deng, Y. Wang, Y. Wang, Ceram. Int. 40 (2014) 8093–8101.
[29] S. Gnanam, V. Rajendran, J. Alloys Compd. 550 (2013) 463–470.
[30] G. Panthi, A. Yousef, N.A.M. Barakat, K.A. Khalil, S. Akhter, Y.R. Choi, H.Y. Kim, Ceram. Int. 39 (2013) 2239–2246.
[31] M.T. Qamar, M. Aslam, I.M.I. Ismail, N. Salah, A. Hameed, ACS Appl. Mater. Interfaces 7 (2015) 8757–8769.
[32] M.T. Qamar, M. Aslam, I.M.I. Ismail, N. Salah, A. Hameed, Chem. Eng. J. 283 (2016) 656–667.
[33] H.Y. Xu, S.L. Xu, X.D. Li, H. Wang, H. Yan, Appl. Surf. Sci. 252 (2006) 4091–4096.
[34] N. Li, J.-Y. Wang, Z.-Q. Liu, Y.-P. Guo, D.-Y. Wang, Y.-Z. Su, S. Chen, RSC Adv. 4 (2014) 17274–17281.
[35] W. Qian, Z. Chen, S. Cottingham, W.A. Merrill, N.A. Swartz, A.M. Goforth, T.L. Clare, J. Jiao, Green Chem. 14 (2012) 371–377.
[36] J. Philip, N. Theodoropoulou, G. Berera, J.S. Moodera, B. Satpati, Appl. Phys. Lett. 85 (2004) 777–779.
[37] G. Singh, A. Choudhary, D. Haranath, A.G. Joshi, N. Singh, S. Singh, R. Pasricha, Carbon 50 (2012) 385–394.
[38] M. Aslam, M.T. Qamar, Z.A. Rehan, M.T. Soomro, M.W. Ashraf, I.M.I. Ismail, A. Hameed, RSC Adv. 6 (2016) 2436–2449.
[39] M. Aslam, M.T. Soomro, I.M.I. Ismail, H.A. Qari, M.A. Gondal, A. Hameed, RSC Adv. 5 (2015) 102663–102673.
[40] P. Pichat, Photocatalysis and Water Purification: From Fundamentals to Recent Applications, 1st ed., Wiley-VCH Verlag GmBH, Germany, 2013.
[41] Y. Li, J. Niu, L. Yin, W. Wang, Y. Bao, J. Chen, Y. Duan, J. Environ. Sci. 23 (2011) 1911–1918.
[42] Heterogeneous Photocatalysis Using Inorganic Semiconductor Solids, in: U.I. Gaya (Ed.), 1st ed., Springer, Dordrecht, The Netherlands, 2014.
[43] M. Aslam, M.T. Qamar, M.T. Soomro, I.M.I. Ismail, N. Salah, T. Almeelbi, M.A. Gondal, A. Hameed, Appl. Catal. B Environ. 180 (2016) 391–402.
[44] B.G. Kwon, J. Yoon, Bull. Korean Chem. Soc. 30 (2009) 667–670.
[45] A. Boudjemaa, S. Boumaza, M. Trari, R. Bouarab, A. Bouguelia, Int. J. Hydrogen Energy 34 (2009) 4268–4274.
[46] D. Hwang, J. Kim, T. Park, J. Lee, Catal. Lett. 80 (2002) 53–57.
[47] Y. Xu, M.A.A. Schoonen, Am. Mineral. 85 (2000) 543–556.
[48] M. Aslam, M.T. Soomro, I.M.I. Ismail, N. Salah, M.A. Gondal, A. Hameed, J. Environ. Chem. Eng. 3 (2015) 1901–1911.